

2-D ELECTROMAGNETIC MODEL OF FAST-RAMPING SUPERCONDUCTING MAGNETS

B. Auchmann, R. de Maria, S. Russenschuck, CERN, Geneva, Switzerland
 S. Kurz, ETAS GmbH, Stuttgart, Germany

Abstract

Fast-ramping superconducting (SC) accelerator magnets are the subject of R&D efforts by magnet designers at various laboratories. They require modifications of magnet design tools such as the ROXIE program at CERN, i.e. models of dynamic effects in superconductors need to be implemented and validated. In this paper we present the efforts towards a dynamic 2-D simulation of fast-ramping SC magnets with the ROXIE tool. Models are introduced and simulation results are compared to measurements of the GSI001 magnet of a GSI test magnet constructed and measured at BNL.

INTRODUCTION

The ROXIE program was conceived for the design of superconducting (SC) magnets [?]. The coil fields are calculated from the Biot-Savart formula and the yoke fields are determined using a coupling method of finite elements and boundary elements. In addition, a model for persistent-currents (PCs) based on the critical state model is implemented for the simulation of SC magnets under DC conditions.

For the simulation of fast-ramping magnets additional eddy-current related effects need to be modeled. In this paper we present 2-D simulations of a SC magnet. Eddy currents in the laminated yoke, which occur mainly in the 3-D end region of a magnet, are neglected. Eddy currents in the SC coils, however, are considered. Models for inter-filament coupling currents (IFCCs) and inter-strand coupling currents (ISCCs) are implemented in ROXIE.

For the FAIR-project (Facility for Antiproton and Ion Research) at the "Gesellschaft für Schwerionenforschung" (GSI), a model dipole called GSI001 was built at Brookhaven National Laboratory (BNL), with a nominal field of 4 T and ramp rates of up to 4 T/s. The magnet design is similar to an existing dipole at BNL, with some changes for loss reduction and improved cooling. The magnet length is approximately 1.2 m. Measurements of field quality and losses have been carried out at BNL at different ramp rates [?].

We present a comparison of simulations and measurements of the GSI001 dipole with ROXIE, as well as the mathematical models involved.

EDDY CURRENT EFFECTS IN SC COILS

In this section we present the mathematical models for persistent currents, inter-filament coupling currents, and

inter-strand coupling currents.

Persistent Currents

According to the critical state model by Bean [?] the (persistent) currents that shield the inside of a Type-II superconducting slab always flow at the critical current density J_c of the material, Fig. 1 (top). Wilson [?] applied the critical state model to a circular cylinder in a transverse field to describe persistent currents in filaments. Aleksa et al. [?] refined the Wilson model in order to account for the inhomogeneous critical current density inside one layer of shielding currents. The inhomogeneity is due to the fact that J_c depends on the local magnetic induction. The shielding effects of the outermost currents need to be taken into account in the calculation of J_c further inside, Fig. 1 (bottom).

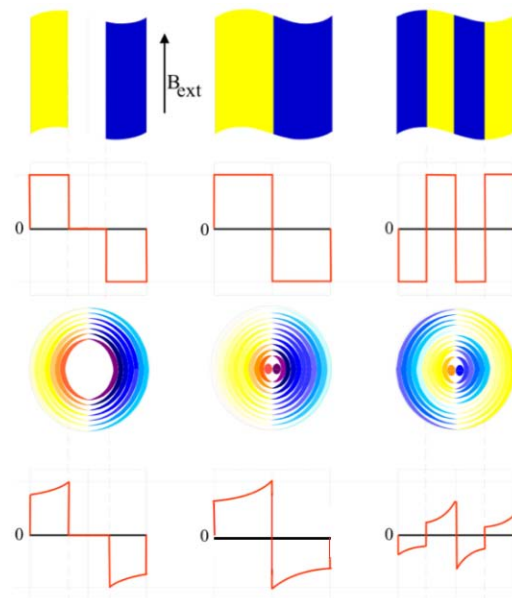


Figure 1: Top: Shielding currents according to the critical state model in a SC slab with parallel external field. Bottom: Shielding currents according to the refined critical state model in round filaments. In the left plots the external field is increased from zero to an external induction B_{ext} . In the middle plot, the field is further increased until it fully penetrates the SC material. In the right plot the field is decreased again, inducing a new layer of shielding currents.

The magnetization of one layer of shielding currents be-

tween normalized radii q_i and q_{i+1} is calculated by

$$\begin{aligned} M_{PC,i} &= \lambda_f \frac{4r}{\pi} \int_{q_i}^{q_{i+1}} J_c(B(q), T) (1-q)^2 dq \\ &\approx \lambda_f \frac{4r\mathcal{F}}{\pi} \int_{q_i}^{q_{i+1}} \frac{(1-q)^2}{\sqrt{B(q)}} dq, \end{aligned}$$

where $\mathcal{F} = J_c(B_{\text{ext}}, T) \sqrt{B_{\text{ext}}}$ with the B_{ext} the magnetic induction outside the filament, r is the filament radius, and λ_f is the filling factor of filaments in a strand [?].

Inter-filament Coupling Currents

The filaments in a strand are twisted with a characteristic twist pitch $L_{p,s}$. The filaments are imbedded in a matrix with an effective resistivity ρ_{eff} . Eddy currents are induced in loops of a length of up to half a twist pitch, bounded by the superconducting filaments and closed across the resistive matrix, Fig. 2. The resulting magnetization produced

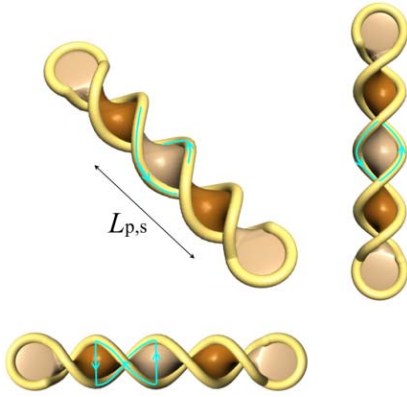


Figure 2: Eddy-current loop between two twisted filaments in a resistive matrix. Visualization with SeifertView [?].

by eddy currents in these loops can be calculated [?]

$$M_{IF} = \lambda_s \partial_t B \frac{L_{p,s}}{2\pi} \frac{1}{\underbrace{\rho_0 + \rho_1 B}_{\rho_{\text{eff}}}},$$

where λ_s is the filling factor of twisted filaments in a strand, ρ_0 is the constant part of the effective resistivity and ρ_1 the slope of the magneto-resistive effect.

Inter-strand Coupling Currents

Inter-strand coupling currents (ISCCs) in Rutherford-type conductors are the equivalent effects to IFCCs on the strand level. On the scale of half a conductor twist-pitch we find loops that are bounded by superconducting strands and cross- and adjacent resistances. In order to consider all relevant loops we model the Rutherford cable as an electrical network [?], Fig. 3. The sources in the electrical network are the time derivatives of the integrated magnetic vector potential along the branches of the network. With $[M]$ the

mesh matrix of the network and $[R]$ the resistance matrix, $\{I\}$ the branch currents and $\{\partial_t A\}$ the induced voltage, we can solve for the currents by evaluating

$$\{I\} = -[M]([M][R][M]^T)^{-1}[M]\{\partial_t A\}.$$

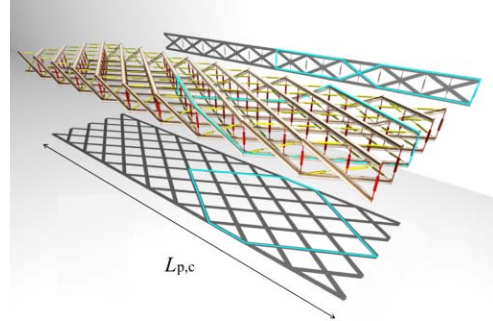


Figure 3: Electrical network representing one twist-pitch length of a Rutherford-type cable. Adjacent resistances between neighboring strands are depicted in yellow and cross-over resistances in red.

SIMULATION OF GSI001

The GSI001 magnet was built from a slightly adapted RHIC coil design. The Rutherford-type cable is wound around a 25 μm stainless-steel core in order to increase the cross-over resistance and reduce ISCCs. The GSI001 dipole was powered between 0 and 4 T central field with ramp rates varying from 0 to 4 T/s.

To analyze the contribution of each of the above effects to the field distortions we look at the difference in the absolute sextupole component (in tesla) between up- and down-ramp of an excitation cycle. The multipole content is analyzed at a reference radius r_0 of 25 mm, according to the Fourier decomposition of the radial component of the magnetic induction in the aperture

$$B_r(r, \varphi) = \sum_{n=1}^{\infty} \left(\frac{r}{r_0}\right)^{n-1} (B_n \sin n\varphi + A_n \cos n\varphi).$$

Measurement data of GSI001 was supplied in [?].

Signatures in the ΔB_3 Plot

PCs and IFCCs have a similar signature in the ΔB_3 plot, which shows the difference in the absolute sextupole component between up- and down-ramp, see Fig. 4. Both effects are inversely proportional to the magnetic induction. For PCs this is due to the critical current density in superconductor, and for IFCCs the reason lies in the magneto-resistance of the resistive matrix. Of course, only IFCCs depend linearly on the ramp rate. ISCCs have a different signature. Their contribution to the ΔB_3 plot has opposite sign. Surprisingly, also the ISCC contribution reduces

with the magnetic induction! To understand this effect we have to observe that the ISCCs fade away when iron saturation sets in. At this point the global field configuration across the coils changes. The centre of the magnetic flux lines moves into the coil cross-section, thus reducing the net flux through the broad side of the cables, Fig. 5.

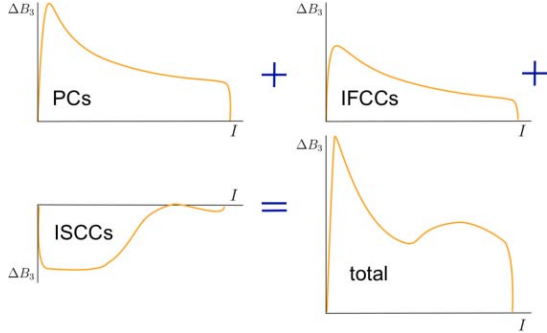


Figure 4: Typical signatures in the ΔB_3 graph of PCs, IFCCs, and ISCCs.

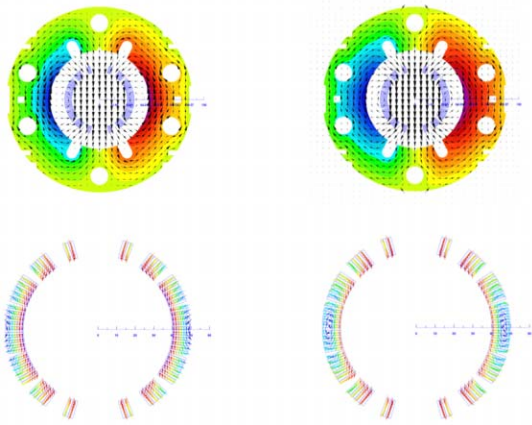


Figure 5: Distribution of magnetic flux in the GSI001 magnet at low excitation (left) and high excitation (right). At low excitation the highly permeable yoke pulls the centre of the magnetic flux lines from the coils towards the yoke. At high saturation the vertex moves back into the coil.

Simulation with Nominal Material Parameters

We give the nominal material parameters [?] of the above models and show the comparison of measurements and simulation results of the GSI001 magnet.

The critical current density as a function of the temperature T and the modulus of the magnetic induction $B = |\mathbf{B}|$ is given by the following fit [?], where $B_c = B_{c20}(1 - (T/T_{c0})^{1.7})$

$$J_c(B, T) = \frac{J_c^{\text{ref}} C_0 B^{\alpha-1}}{(B_c)^\alpha} \left(1 - \frac{B}{B_c}\right)^\beta \left(1 - \left(\frac{T}{T_{c0}}\right)^{1.7}\right)^\gamma$$

with parameters for Nb-Ti of $J_c^{\text{ref}} = 3 \cdot 10^9 \text{ Am}^{-2}$, $B_{c20} = 14.5 \text{ T}$, $T_{c0} = 9.2 \text{ K}$, $C_0 = 27.04 \text{ T}$, $\alpha = 0.57$, $\beta = 0.9$, and $\gamma = 2.32$. The filament diameter is $6 \mu\text{m}$ and the non-superconductor ratio in the strand is 2.21. The parameters for IFCCs are $\rho_0 = 1.24 \cdot 10^{-10} \Omega\text{m}^{-1}$, $\rho_1 = 9 \cdot 10^{-9} \Omega\text{m}^{-1}\text{T}^{-1}$, and $\lambda_s = 0.5$, with a twist-pitch length $L_{p,s} = 4 \text{ mm}$. The ISCC model uses the following parameters: number of strands per conductor 30, twist-pitch length 74 mm, $R_a = 6.4 \cdot 10^{-5} \Omega$, and $R_c = 6.25 \cdot 10^{-2} \Omega$. Results obtained with these parameters are shown in Fig. 6.

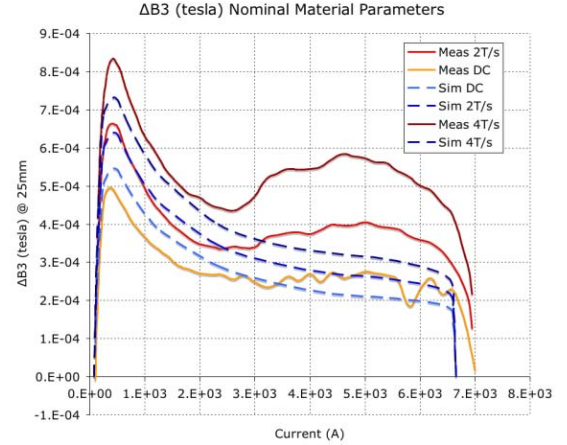


Figure 6: Difference in the absolute sextupole (in tesla) between up- and down ramp between 0 and 4 T in the aperture of the GSI001 dipole at DC conditions, 2 T/s, and 4 T/s ramp rates. Measurement results are shown in red, simulations in blue with dashed lines. Simulations use nominal material parameters.

Simulation with Adapted Material Parameters

Some effort was put into the reconstruction of the measured ΔB_3 curves at 0, 2, and 4 T/s. We present the parameters that reproduce the measurements reasonably well. For the DC curve a different critical current fit was required, as the flat curve in the high-field region could not be reproduced with the above function. The fit reads [?]

$$J_c(B, T) = J_c^{\text{ref}} C_0 (C_1 e^{-B\alpha_1} + 1) (C_2 e^{-B\alpha_2} + 1) \left(1 - \frac{B}{B_c}\right)^\beta \left(1 - \left(\frac{T}{T_{c0}}\right)^{1.7}\right)^\gamma, \quad (1)$$

with B_c defined above and with the parameters $J_c^{\text{ref}} = 3 \cdot 10^9 \text{ Am}^{-2}$, $B_{c20} = 14.5 \text{ T}$, $T_{c0} = 9.2 \text{ K}$, $C_0 = 6.5$, $C_1 = 2$, $C_2 = 2$, $\alpha_1 = 6 \text{ T}^{-1}$, $\alpha_2 = 15 \text{ T}^{-1}$, $\beta = 0.5$, and $\gamma = 2.32$. For IFCCs we use $\rho_0 = 9 \cdot 10^{-11} \Omega\text{m}^{-1}$, $\rho_1 = 3 \cdot 10^{-11} \Omega\text{m}^{-1}\text{T}^{-1}$, $\lambda_s = 0.7$. The ISCC resistances are set to $R_a = 1.8 \cdot 10^{-5} \Omega$, and $R_c = 6.25 \cdot 10^{-2} \Omega$. Results from these parameters are shown in Fig. 7.

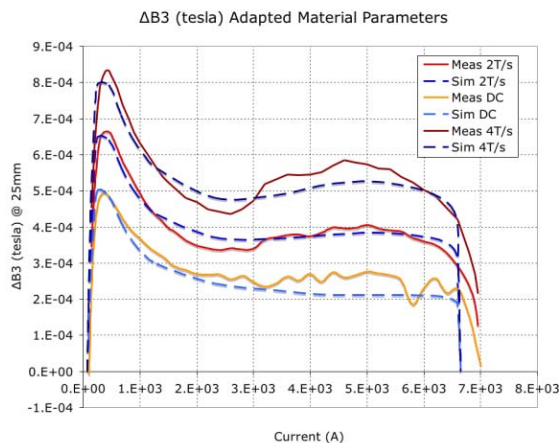


Figure 7: Difference in the absolute sextupole (in tesla) between up- and down-ramp between 0 and 4 T in the aperture of the GSI001 dipole at DC conditions, 2 T/s, and 4 T/s ramp rates. Measurement results are shown in red, simulations in blue with dashed lines. Simulations use adapted material parameters in order to better reproduce the measurements.

Table 1: Losses per ramp cycle in J/(m cycle).

Ramp-Rate	Meas.	Sim. Nominal	Sim. Adapt.
DC	40	28.5	27.5
2 T/s	83	42.5	69.3
4 T/s	126	56.5	108.7

DIFFICULTIES IN SIMULATION

Although the above results look promising, there are other measured quantities such as decapole- and skew quadrupole components that cannot be predicted with the models.

Losses

The measured and calculated losses are summarized in Tab. 1. It can be seen that the ramp-rate dependent losses due to eddy currents in conductive material are well predicted in the adapted model. The difference between measured and simulated DC losses is not unexpected due to the iron hysteresis losses which are not included in the present model.

The ΔB_5 Curve

Although the results from adapted material parameters reproduce the ΔB_3 curve reasonably well, the comparison of measurement- and simulation results for the ΔB_5 curves point to an additional ramp-rate dependent effect in GSI001, compare Fig. 8.

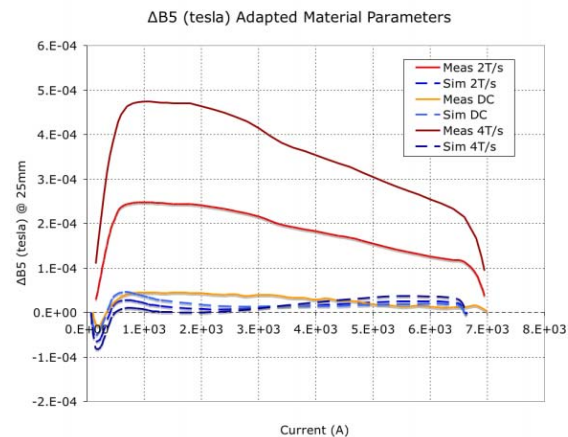


Figure 8: Difference in the absolute decapole (in tesla) between up- and down-ramp between 0 and 4 T in the aperture of the GSI001 dipole at DC conditions, 2 T/s, and 4 T/s ramp rates. Measurement results are shown in red, simulations in blue with dashed lines. Simulations use adapted material parameters in order to better reproduce the measurements.

Reproducing ΔA_2

Similarly, measurements show a ramp-rate dependent skew quadrupole component, which is zero in DC conditions and which cannot be simulated in the above model due to an up-down symmetry in geometrical and material parameters.

In an attempt to reproduce the skew quadrupole in transient conditions, we simulate a cross-section built from two different coils. The upper coil has an adjacent resistance of $R_a = 1.8 \cdot 10^{-5} \Omega$, whereas the lower coil has $R_a = 1.0 \cdot 10^{-5} \Omega$. Figure 9 shows the ΔA_2 curve for simulations and measurements at 2 T/s and Fig. 10 shows the corresponding pattern of interstand coupling currents in the coil cross-section.

Radial Dependence of R_a

Aiming for a deeper understanding of transient effects in the GSI001 we also tested the impact of an adjacent resistance that rises linearly with the radial distance from the center. R_a on the inner and outer cable edge varied between $1.0 \cdot 10^{-5} \Omega$ and $2.8 \cdot 10^{-5} \Omega$. The losses, as well as the impact on field quality remained equivalent to the above presented simulations with homogeneous adjacent resistance of $1.3 \cdot 10^{-5} \Omega$.

CONCLUSION AND OUTLOOK

We list our observations from the simulation of GSI001:

- The DC signature in the ΔB_3 graph ends on a flat plateau for high fields. This measurement result cannot be explained by a superconducting material with

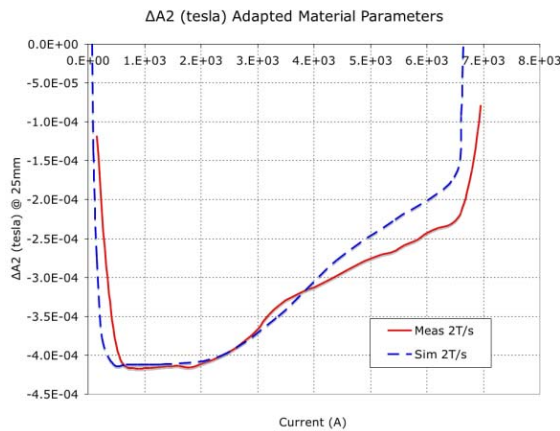


Figure 9: Difference in absolute skew quadrupole (in tesla) between up- and down-ramp between 0 and 4 T in the aperture of the GSI001 dipole at 2 T/s ramp rate. Measurement results are shown in red, simulations in blue with dashed lines. For the simulation the adjacent resistance in the upper coil was set to $R_a = 1.8 \cdot 10^{-5} \Omega$ and the lower coil was set to $R_a = 1.0 \cdot 10^{-5} \Omega$.

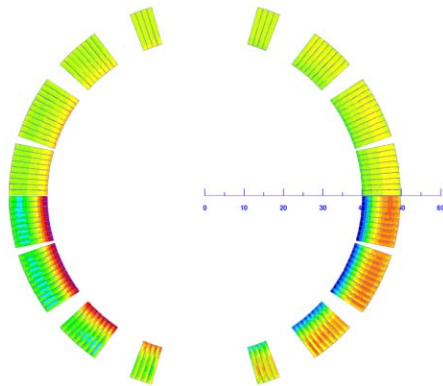


Figure 10: ISCCs in the cross-section of GSI001 coils for unsymmetric adjacent resistance in upper and lower coil. For the upper coil $R_a = 1.8 \cdot 10^{-5} \Omega$ and for the lower coil $R_a = 1.0 \cdot 10^{-5} \Omega$.

nominal parameters

$$J_c(5.5 \text{ T}, 4.2 \text{ K}) = 2.5 \cdot 10^9 \text{ Am}^{-2} \text{ and}$$

$$dJ_c/dB(5.5 \text{ T}, 4.2 \text{ K}) = 0.58 \cdot 10^9 \text{ Am}^{-2} [?].$$

The adapted J_c fit above does not reproduce these parameters, whereas the fit used for nominal calculations approximately does.

- The DC losses from PCs are smaller than the measured ones. The missing losses are assigned to hysteresis effects in the yoke iron.
- The adapted parameters for IFCCs and ISCCs allow to reproduce reasonably well the ΔB_3 graphs for different ramp rates. The parameters, in particular for

IFCCs, however, are unlikely to be found in superconducting cable. The IFCC resistivities are extremely small.

- The ramp-rate dependent losses in the adapted model reproduce the measured ramp-rate dependent losses. However, it should be expected that ramp rates up to 4 T/s induce eddy currents also in the laminated yoke, in particular in the end region. The predicted IFCC- and ISCC-losses are therefore probably too high.
- The presented models do not account for the ΔB_5 graph in AC conditions. An additional effect is required to explain the decapole graphs.

At this point we must conclude that a full understanding of the dynamic effects in GSI001 has not yet been reached. Further steps could be the simulation of hysteresis effects in the yoke, as well as of 3-D eddy current effects in the end regions. Measurements of a longer magnet would be better suited to identify different effects.